Phase Evolution and Spinodal Decomposition in Ti-13Mo-2Fe During Aging

M.G. DE MELLO, C.A.F. SALVADOR, F.H. COSTA, K.N. CAMPO, C.R.M. AFONSO, A. CREMASCO, and R. CARAM

This paper investigates the phase formation in Ti-13Mo-2Fe (wt pct) during aging. Ti-13Mo-2Fe prevented athermal ω formation after solution treatment. However, the high diffusivity of Fe favored isothermal ω formation and growth during aging. Furthermore, a secondary BCC phase was detected in the aged sample. The isothermal ω generates Mo- and Fe-enriched regions that may drive the spinodal decomposition of the parent β at 400 °C. The simulation showed a good agreement with the experimental data.

https://doi.org/10.1007/s11661-024-07601-7

β-Ti alloys are extensively used in several industrial sectors due to their versatile mechanical properties. It is well known that their mechanical strength can be increased through controlled α precipitation into the β matrix.[1,2] The most common mechanism for α formation is classical nucleation based on heterogeneous sites. Several studies have shown that nucleation sites are related to both structural differences (such as grain boundaries or low coherence between crystal structures) and compositional variations.[3–5] Regarding the latter, spinodal decomposition is a phase transformation that leads to phase separation ($\beta \rightarrow \beta + \beta'$). It occurs when a miscibility gap is associated with the alloy composition and does not depend on an interface or nucleation stage.[6] The spinodal decomposition products are phases with a structure similar to that of the parental phase (or a very similar one) but with dissimilar compositions. They can be strongly involved in the ω or α formation. For instance, Zhu *et al.*[7] observed that α precipitates nucleate at the β/β' interface and grow into the solute-lean regions. Spinodal decomposition has been reported to occur in some Ti-based alloys.[8,9] In this study, we provide experimental evidence of phase separation in Ti-13Mo-2Fe (wt pct), which is further supported by thermodynamic/kinetics simulations. These findings are significant in clarifying the effects of Fe on the phase transformations of Ti–Mo alloys. Fe is a low-cost beta-stabilizer that decreases the beta-phase lattice parameter, increases omega solvus, and enables higher mechanical strengths.[10]

To prepare the Ti-13Mo-2Fe (wt pct) alloy, an arc-melted ingot was homogenized at 1000 °C for 24 hours, hot rolled, solution heat-treated at 1000 °C for 1 hour, water quenched, and aged at 400 °C for 24 hours. Microstructural analysis was conducted using X-ray diffraction (XRD—PANalytical X-Pert Pro, Cu-K_α radiation) combined with Rietveld refinement data using GSAS program suite. Ytria powder was employed as a reference to obtain the XRD instrument calibration file. Transmission electron microscopy was also used, including a JEOL JEM 2100 operating at 200 kV and a Cs-corrected FEI TITAN Themis Cubed operating at 300 kV TEM/STEM, equipped with ChemiStem EDS detectors. TEM specimens were prepared using disc punching, dimpling, and argon ion milling with a Gatan precision ion polishing system. Simulation tools, ThermoCalc® and DICTRA, were also employed to determine the equilibrium phase fractions and to simulate the formation of the α phase.

The TEM-SAD pattern of the solution-treated Ti-13Mo-2Fe sample shows only the presence of the β phase (Figure 1(a)). XRD analysis (Figure 1(b)) determined the β lattice parameter to be 0.3245 nm, compared to 0.3263 nm for the binary Ti-13Mo (wt pct) alloy.[11] Typically, the absence of athermal ω (ω_{ath}) after quenching is achieved when the Mo content is approximately 15 wt pct.[12] Since the ternary alloy used here has an equivalent Mo content of 18 wt pct, this explains the suppression of ω_{ath}. However, this

M.G. DE MELLO is with the School of Mechanical Engineering, University of Campinas, Campinas, SP 13083-860, Brazil and also with the School of Applied Sciences, University of Campinas, Limeira, SP 13484-350, Brazil. C.A.F. SALVADOR is with the University of Grenoble Alpes, CNRS, Grenoble INP, SIMAP, 38000 Grenoble, France. F.H. COSTA, K.N. CAMPO, and R. CARAM is with the School of Mechanical Engineering, University of Campinas. C.R.M. AFONSO is with the Department of Materials Engineering, Federal University of São Carlos, São Carlos, SP 13564-905, Brazil. A. CREMASCO is with the School of Applied Sciences, University of Campinas. Contact e-mail: acremasc@unicamp.br
Manuscript submitted May 23, 2024; accepted September 19, 2024.
Article published online October 3, 2024

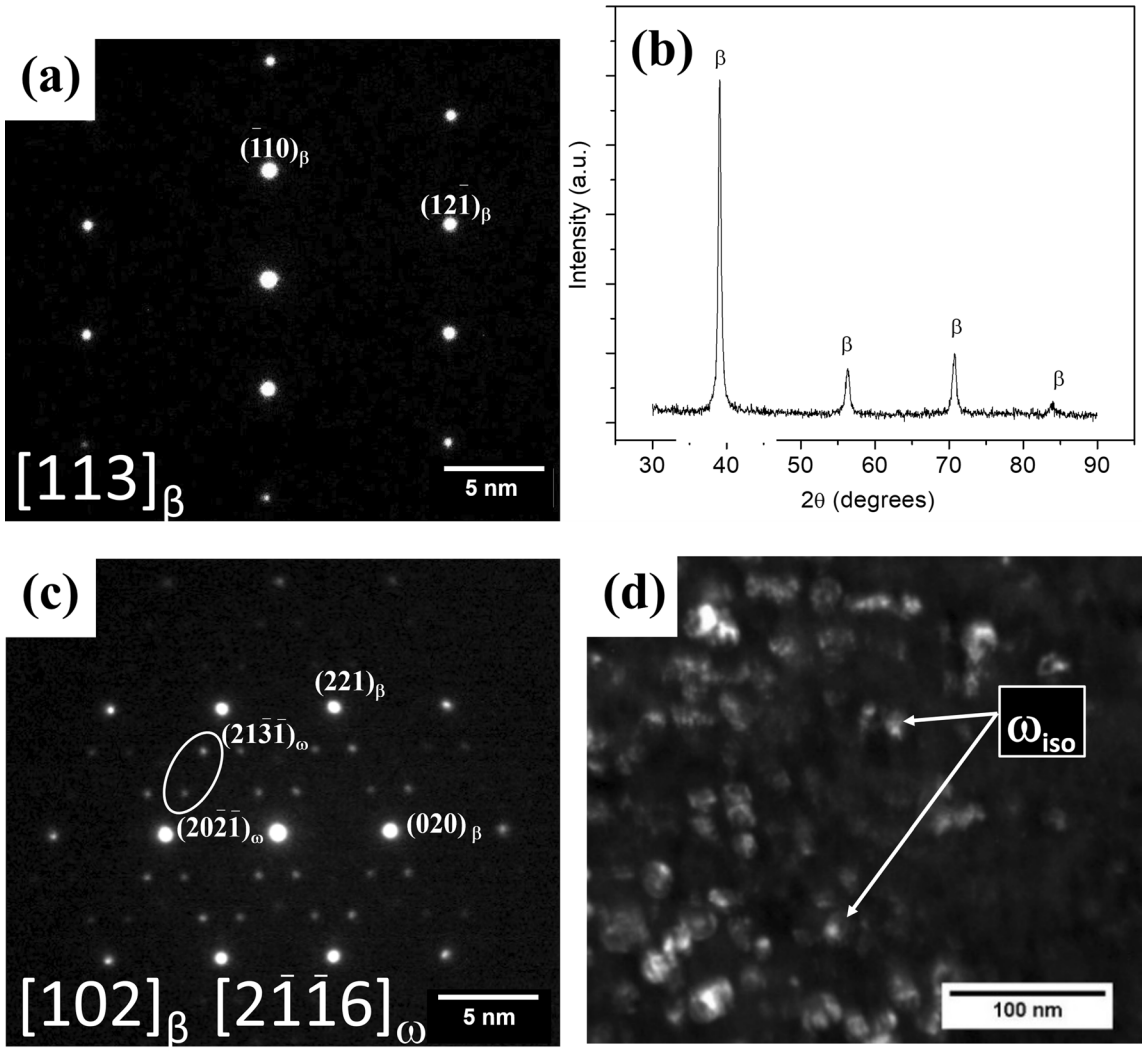

Fig. 1—SADP-TEM and XRD pattern of Ti-13Mo-2Fe: (*a*, *b*) after solution treatment and water quenching, and SADP-TEM and DF image obtained from circled reflections (*c*, *d*) after aging at 400 °C for 24 h.

threshold does not always hold, as demonstrated by the observation of ω_{ath} particles in a binary Ti-18Mo (wt pct).[13] This highlights the strong ω_{ath} suppression effect of Fe. It is generally acknowledged that a decrease in the β lattice parameter facilitates the collapse of the $\{111\}\beta$ planes, thereby favoring the formation of ω_{ath}.[10] However, the addition of Fe favors the formation of Fe–Fe, Mo–Fe, and Ti–Fe chemical bonds over Ti–Ti bonds, resulting in a new electron density configuration that alters phase transformation behavior.[14] After aging at 400 °C for 24 hours, the TEM results of SAD Pattern in Figure 1(c) and Dark-Field (DF) image in Figure 1(d) reveal that the microstructure is composed of β and isothermal ω (ω_{iso}). This temperature is too low to induce α precipitation but allows the growth of ω_{iso} precipitates. The β matrix and ω variants diffraction spots were indexed with the aid of CrystTBox.[15]

A deeper characterization of ω_{iso} precipitation was performed through STEM analysis (Figure 2). In Ti–Mo binary alloys, ω precipitates are typically ellipsoidal due to the low misfit between ω and β.[16] However, in the Ti–Fe system, the high misfit between these phases leads to the formation of cuboidal ω.[17] Nevertheless, the addition of only 2 wt pct Fe was insufficient to change the ω morphology, as shown in Figure 2(a). These ellipsoidal precipitates, with average semi-axes Ra $\approx$ 26 nm and Rb $\approx$ 19 nm, are depleted in both Mo and Fe, indicating that ω is a precursor to equilibrium α precipitation, rejecting β-stabilizing elements and becoming richer in Ti. A higher magnification STEM-HAADF was used to carefully examine the solute distribution in the β matrix after aging (Figure 2(b)). The Z-contrast image and STEM mapping clearly depict the contrast and phase separation between the β (dark) and β' (bright) phases. Table I presents the semi-quantitative compositional analysis, indicating that the main compositional difference is related to the Mo content. Although the β' phase appears to be slightly richer in Fe, the mean values for Fe content are not statistically different ($p > 0.05$). The third line in Table I (alloy) represents a general EDS

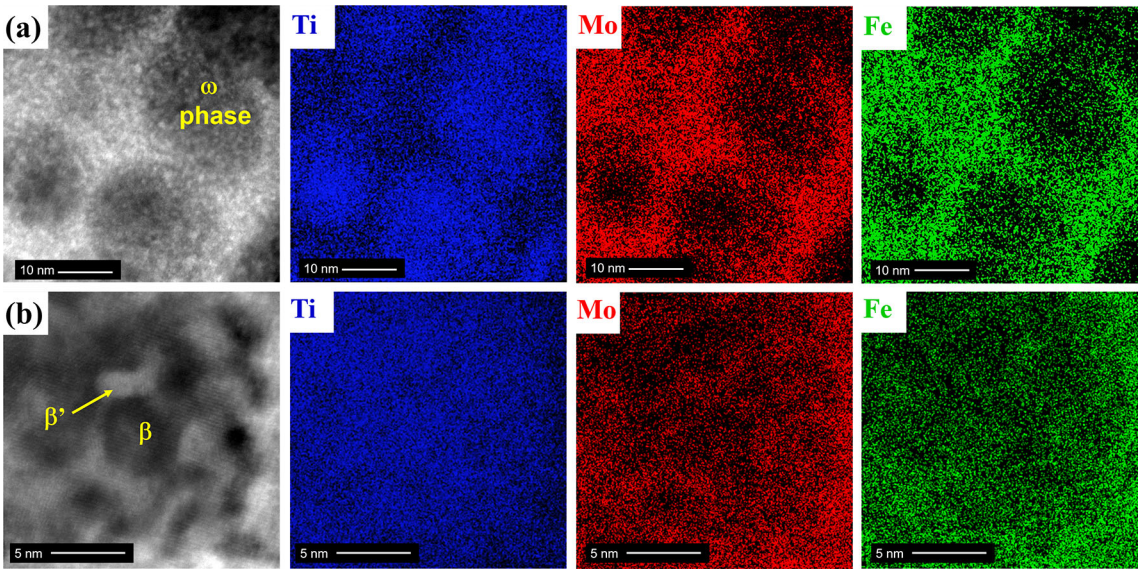

Fig. 2—STEM analysis of Ti-13Mo-2Fe aged at 400 °C for 24 h: (*a*, *b*) HAADF (Z-contrast) images with corresponding EDS elemental mapping at different magnifications.

Table I. Chemical Semi-quantitative Analysis (EDS-STEM) of Ti-13Mo-2Fe Aged for 24 h at 400 °C

Phase	Ti (wt pct)	Mo (wt pct)	Fe (wt pct)
β	Balance	9.2 ± 1.4	1.5 ± 0.2
β'	Balance	14.9 ± 0.1	1.9 ± 0.3
Alloy	Balance	12.7 ± 0.3	1.8 ± 0.2

analysis conducted at low magnification in the TEM. This analysis was performed over a large area of the sample to obtain an average composition, which serves as a reference.

Devaraj *et al.*[13] investigated phase separation and ω precipitation in Ti-18Mo (wt pct) and found that compositional clustering occurred during rapid cooling from the β field, resulting in Mo-enriched and Mo-depleted regions. In the Mo-depleted regions, $\{111\}\beta$ planes collapsed, leading to the formation of ω embryos. In contrast, the Ti-13Mo-2Fe alloy, after solution treatment, exhibited a fully β-phase microstructure, with compositional clustering only detected following subsequent aging at 400 °C for 24 hours. This suggests that Ti-13Mo-2Fe is situated between two points of inflection on the free energy curve of the β phase.

Spinodal decomposition differs from classical nucleation and growth because higher supersaturation is required to induce small compositional fluctuations that result in phase separation.[18] The addition of Fe has promoted these compositional fluctuations. Although the interfaces between β and β' structures are not very sharp, they may serve as nucleation sites for ω_{iso}. Consequently, ω_{iso} nucleates in Mo- and Fe-depleted regions, and the growth of these precipitates may further enhance the compositional fluctuations necessary for spinodal decomposition of β. Therefore, a possible phase transformation sequence for this system could be: β matrix $\rightarrow \beta + \omega_{iso} \rightarrow \beta + \beta' + \omega_{iso}$ (in solute-rich regions). However, it is important to note that our experimental data do not distinguish whether ω_{iso} nucleation or spinodal decomposition occurs first. At higher temperatures or longer times, the α-phase formation would become more favorable, replacing ω_{iso}.

The equilibrium phase fractions in the Ti–Mo–Fe system were determined using ThermoCalc® with the TCTI3 database (Figure 3(a)). The normalized driving force (NDF) for the precipitation of β' (BCC_B2#2) from the β matrix (BCC_B2#1) was calculated at different Mo and Fe contents (Figure 3(b)). A positive normalized driving force (NDF) indicates that the precipitation of the Fe-rich BCC phase is feasible. To simulate the α (HCP_A3) formation during aging at 400 °C, we employed DICTRA via the TC-Python module (version 2022b). A planar geometry containing a 500 nm β matrix and a 10 nm α nucleus on the right side was used as the initial system. The compositions of the phases at the beginning of the simulation were set to their equilibrium values at 400 °C. The kinetic simulation was based on SSOL2 and MOB2 databases and was carried out in a closed system with 128 discrete points biased toward the interface.[19,20] The Mo and Fe partitioning over time, with the growth of the α lath, was analyzed, and the results are shown in Figures 3(c) and (d). An accumulation of Mo with contents greater than 30 wt pct is observed near the β/α interface at the beginning of the simulation and persists after 1 hour. In contrast, Fe partitioning decreases over time, given its superior diffusion in the β matrix.

Based on the combined analysis of experiments and simulations, the origins of the solute-rich BCC phase detected in the Ti–Mo–Fe system are difficult to determine. According to the equilibrium calculations, β' should replace the FeTi intermetallic, being the product of a eutectoid decomposition.[21] Figure 3(a) shows the equilibrium volume fraction of this phase is

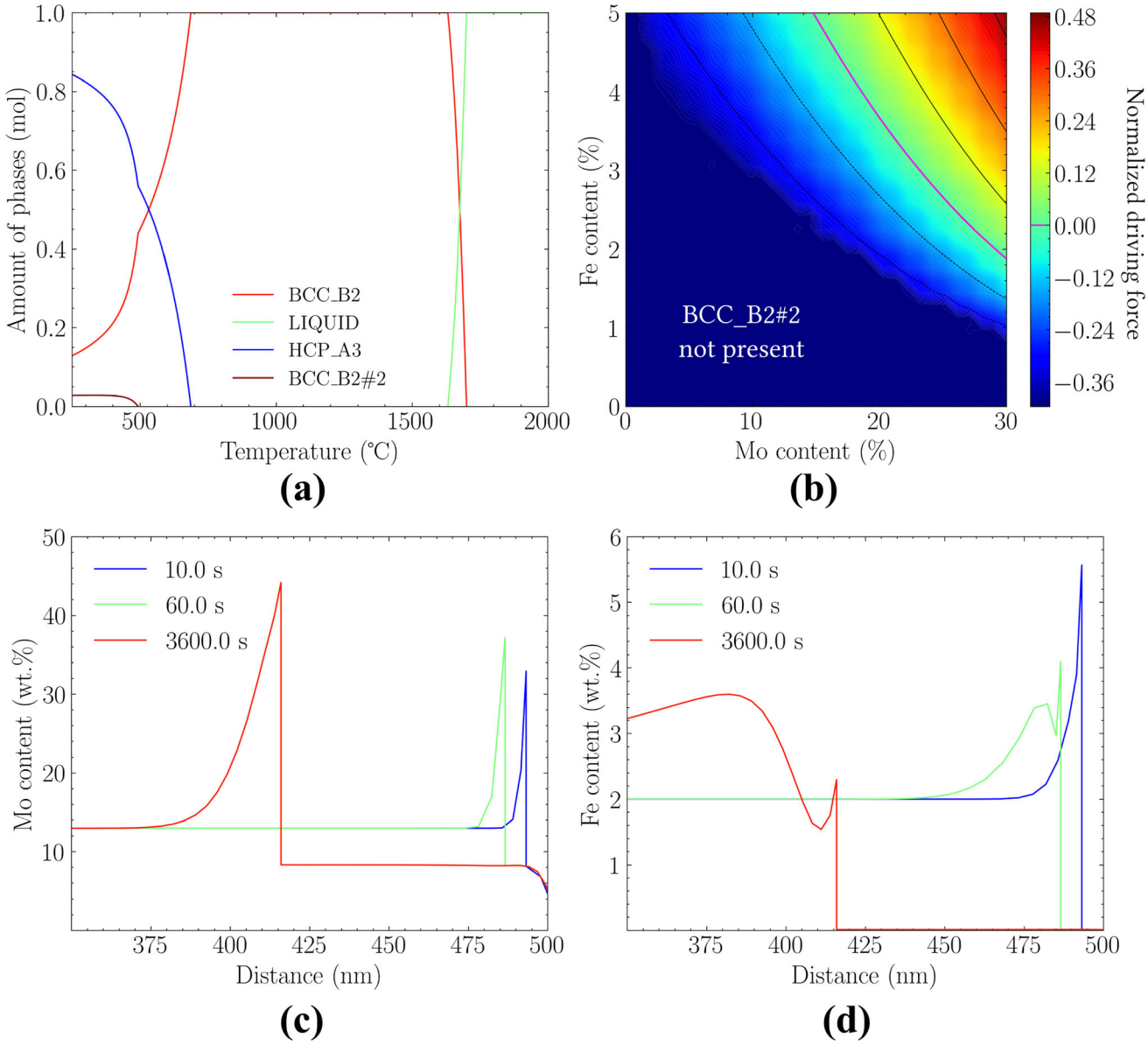

Fig. 3—(*a*) Equilibrium phase fractions and (*b*) normalized driving force (NDF) for the precipitation of β' (BCC_B2#2) from the β matrix (BCC_B2#1), obtained via ThermoCalc®. DICTRA simulations showing the partitioning of (*c*) Mo and (*d*) Fe after 1 hour at 400 °C, based on an initial setup consisting of 500 nm β matrix (left) and 10 nm α lath (right) with 99.7 wt pct Ti.

only 4 pct at 400 °C, with an equilibrium composition of 49.4 wt pct Fe and 5.1 wt pct Mo. In the Ti–Fe system, Zheng *et al.*[22] reported a cubic B2 phase with approximately 50 at pct Fe, particularly in compositions near the Ti–Fe eutectoid line. This phase is also present in the Ti–Mo–Fe system under similar conditions. However, the β' phase observed in our study is fundamentally different. Based on our TEM results and the compositional analysis shown in Table I, the β' phase we detected is only minimally enriched in Fe. This suggests that it follows a distinct formation pathway, likely related to a non-homogeneous transformation mechanism rather than a eutectoid decomposition.

DICTRA simulations suggest that any Ti-rich phase, either ω_{iso} or α, would enable the formation of a solute-rich β at the selected aging temperature, given the pronounced β-stabilizer accumulation at the matrix–precipitate interface (Figures 3(c) and (d)). In such a case, the simulation supports the phase formation evolution sequence proposed above. This suggests that the β to β' transformation may not follow a conventional (sparse) spinodal process but instead occurs in compositional pockets near ω_{iso}, i.e., in solute-rich regions. Sridharan *et al.*[23] observed in Ti-6Al-4V that DICTRA simulations predicted significant V enrichment in the neighboring β phase (up to 18 at pct V) when the α phase grows at 600 °C. Experimental atom probe tomography results indicated even higher V concentrations, up to 25 at pct V near the interface. The authors attributed the discrepancy between simulations and experiments to the exposure of samples to lower temperatures during fabrication, which results in

higher supersaturation and, consequently, increased V content in the β phase. Additionally, the solute-rich BCC phase may form at specific sites, such as crystallographic defects, which provide favorable nucleation conditions and reduce activation energy by approximately 3–6 kJ/mol. The energy shift required for β'-phase formation is minimal, representing less than 2 pct of the typical activation energies for phase transformations in this system.[24]

In summary, the presence of Fe helps avoid the formation of ω_{ath} during quenching. However, its high diffusivity accelerates the formation and growth of ω_{iso} during aging. Consequently, adding Fe led to a large ω_{iso} volumetric fraction, even though the initial microstructure did not contain ω_{ath}. Notably, the presence of a β rich in solutes was linked to the formation of ω_{iso}, as it generates Mo- and Fe-enriched regions that may drive the spinodal decomposition of the parent β. Such regions might also help limit the growth of α precipitates during aging. Kinetic simulations agreed with that hypothesis. While our experimental data indicate the presence of both ω_{iso} and β' phases after aging, the sequence of their formation remains uncertain. Our findings suggest that the β to β' transformation may not follow a conventional spinodal decomposition process. Although this study offers valuable insights into the phase transformations occurring in Ti-13Mo-2Fe during aging, further research is needed to fully elucidate the underlying mechanisms.

ACKNOWLEDGMENTS

We acknowledge FAPESP (#2018/18293-8), CNPq (#407412/2018-2), CAPES/PNPD (#88887.357955/2019-00), and LNNano/CNPEM (TEM facilities).

CONFLICT OF INTEREST

On behalf of all authors, the corresponding author states that there is no conflict of interest.

REFERENCES

1. S.A. Mantri, et al.: *Scr. Mater.*, 2018, vol. 154, pp. 139–44.
2. Y. Zheng, et al.: *Acta Mater.*, 2016, vol. 103, pp. 165–73.
3. Y. Zheng, et al.: *Scr. Mater.*, 2016, vol. 111, pp. 81–4.
4. Y. Zheng, et al.: *SMM*, 2016, vol. 113, pp. 202–05.
5. A. Devaraj, et al.: *Scr. Mater.*, 2013, vol. 69, pp. 513–16.
6. D.A. Porter and K.E. Easterling: *Phase Transformations in Metals and Alloys*, CRC Press, Boca Raton, 2009.
7. Y.M. Zhu, et al.: *Scr. Mater.*, 2016, vol. 112, pp. 46–49.
8. C.R.M. Afonso, et al.: *Acta Biomater.*, 2010, vol. 6, pp. 1625–29.
9. H.P. Ng, et al.: *Acta Mater.*, 2011, vol. 59, pp. 2981–91.
10. C.A.F. Salvador, et al.: *J. Mech. Behav. Biomed. Mater.*, 2017, vol. 89, pp. 162–67.
11. M.G. de Mello, F.H. da Costa, and R. Caram: *MATEC Web Conf.*, 2020, vol. 321, p. 05017.
12. W.D. Zhang, et al.: *Mater Charact*, 2015, vol. 106, pp. 302–07.
13. A. Devaraj, et al.: *Acta Mater.*, 2012, vol. 60, pp. 596–609.
14. D. Choudhuri, et al.: *Acta Mater.*, 2017, vol. 130, pp. 215–28.
15. M. Klinger: *J. Appl. Crystallogr.*, 2017, vol. 50, pp. 1226–34.
16. Y. Zheng, et al.: *Scr. Mater.*, 2016, vol. 123, pp. 81–85.
17. B.S. Hickman: *Met Soc AIME-Trans*, 1969, vol. 245, pp. 1329–36.
18. ASM Metals Handbook 1985.
19. Y. Yang, et al.: *MATEC Web Conf.*, 2020, vol. 321, p. 12011.
20. Thermo-Calc Software General Alloy and Pure Systems version 2 (2022), https://thermocalc.com/products/databases/general-alloys-and-pure-substances/. Accessed Sept 2022.
21. H. Bo, et al.: *Trans. Nonferrous Met. Soc. China*, 2012, vol. 22, pp. 2204–11.
22. Y. Zheng, D. Huber, and H.L. Fraser: *Scr. Mater.*, 2018, vol. 154, pp. 220–24.
23. N. Sridharan, et al.: *J. Mater. Sci.*, 2020, vol. 55, pp. 1715–26.
24. T. Xu, et al.: *Sci. Rep.*, 2019, vol. 9, pp. 1–12.